Supporting Information

Method for Benchmarking Li Metal Anodes: A Mandatory Step toward Reliable Lithium Metal Batteries

Nicolas Delaporte *, Alexis Perea, Mireille Léonard, Julie Matton, Hendrix Demers, Steve Collin-Martin, David Rozon, Daniel Clément, Abdelbast Guerfi and Chisu Kim

Center of Excellence in Transportation, Electrification and Energy Storage, 1806 Bd. Lionel-Boulet, Varennes, QC J3X 1S1, Canada
* Correspondence: delaporte.nicolas@hydroquebec.com (N.D.)

Figure S1 shows the correlation between the relative humidity (%) and the dew point (°C) in the dry room utilized for the exposure of Li strips. A probe is installed beside the assembly exposing the Li foils and it records the dew point for three weeks. Using the equation in Figure S1, valid for a room temperature of 21°C, the corresponding relative humidity can easily be calculated.

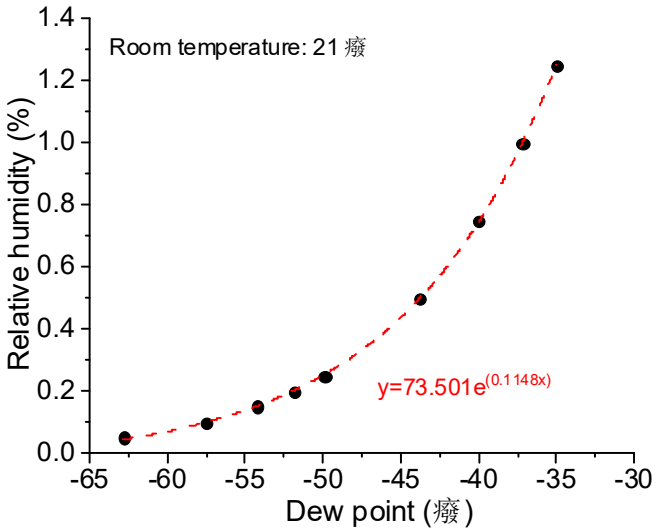

Figure S1. Correlation between the relative humidity (%) and the dew point (°C) in a room temperature of 21°C. The equation can be used to easily convert the dew point temperature into percentage of relative humidity.

Figure S2 presents SEM images and corresponding elemental mappings of b,f,j) Li, c,g,k) C and d,h,l) O for a–d) Lithium HQ, e–h) Lithium #1 and i–l) Lithium #2 (t_0 samples). The composition at the surface of Lithium HQ is the most homogeneous and is mainly composed of Li. The surface of Lithium #1 is highly concentrated in C and O and variations in composition, especially for oxygen, are visible. The white spots (see Figure S2e) are obviously less concentrated in O and C. The surface of Lithium #2 is also highly concentrated in oxygen.

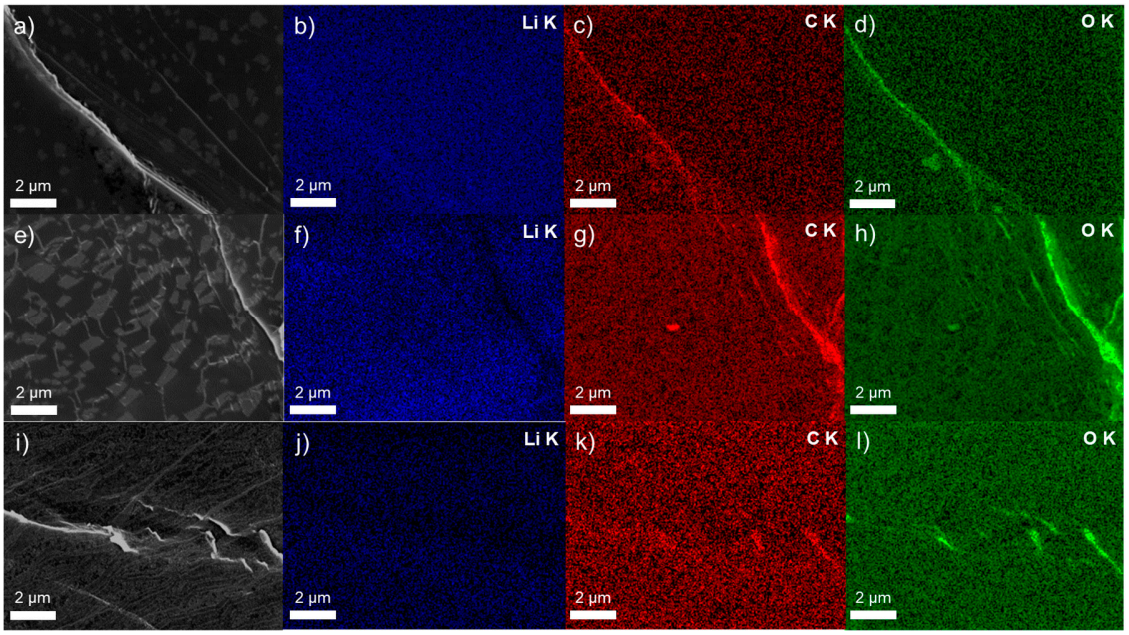

Figure S2. a,e,i) SEM images and corresponding elemental mappings of b,f,j) Li, c,g,k) C and d,h,l) O for a-d) Lithium HQ, e-h) Lithium #1 and i-l) Lithium #2 (t_0 samples). The scale is indicated by the white bars.

Figure S3 shows a,c,e) SEM morphological and b,d,f) composition images for a,b) Lithium HQ and c–f) Lithium #2 foils (t_0 samples). While the surface of the in-house Li appears smooth and homogeneous in composition, although white spots are visible, the surface of Lithium #2 foil is characterized by a strong inhomogeneity in atomic composition. The surface is covered by oxygen-rich spherical particles and cracks revealing fresh Li metal are observed throughout the surface of this sample. A closer look at the Figure S3b (composition image) reveals that the white spots are probably fresh Li or less oxidized Li metal.

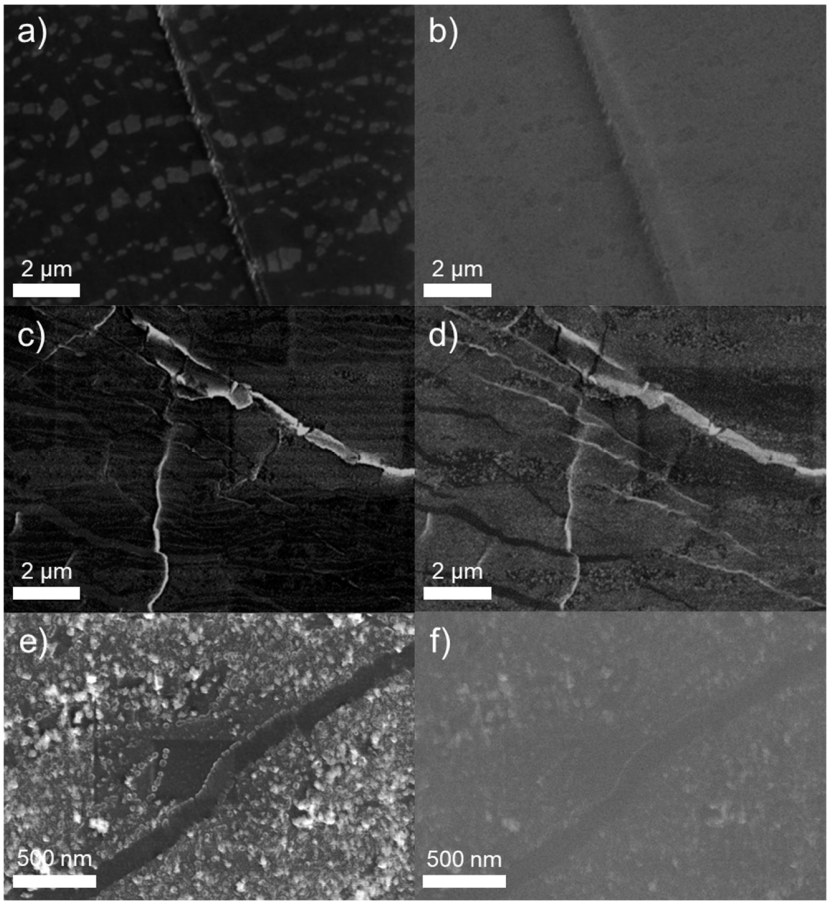

Figure S3. a,c,e) SEM morphological and b,d,f) composition images for a,b) Lithium HQ and c-f) Lithium #2 foils (t_0 samples). The scale is indicated by the white bars.

Figure S4 presents typical EDS spectra acquired on the Li surface (here as an example: Lithium HQ foil exposed during 72 h in dry room). This analysis is performed systematically for all the Li foils exposed for different times in dry room. The data are compiled to follow the evolution of the different atoms' concentration during aging in air (see Figure 2 in the manuscript).

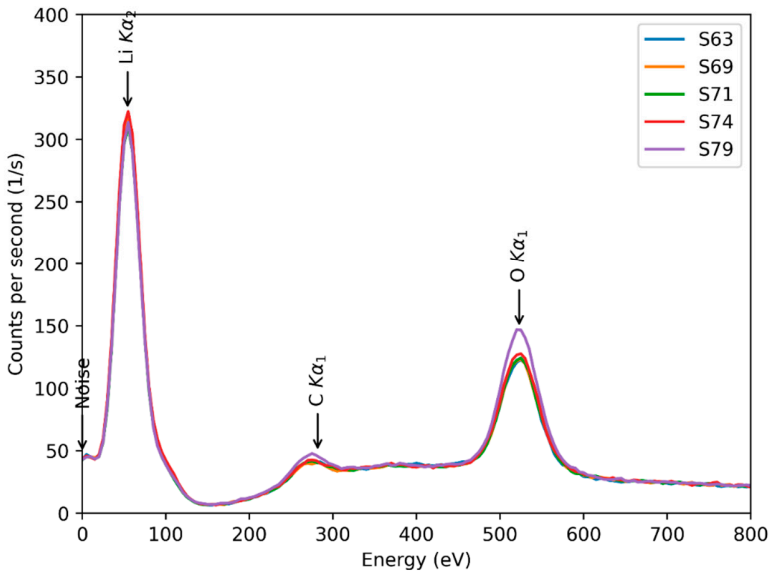

Figure S4. EDS spectra for the Lithium HQ foil exposed during 72 h in dry room. Five measures are made randomly on the Li metal surface.

Optical and 3D laser scanning confocal images of a,b) Lithium HQ, c,d) Lithium #1 and e,f) Lithium #2 surfaces are presented in Figure S5. The indentation mark is clearly visible for Lithium HQ but hardly discernable for the two commercial Li foils, revealing the better surface quality for Lithium HQ. Particularly, 3D laser scanning confocal images show a flat surface for Lithium HQ, with less surface defaults and well drawn Li grain boundaries. Lithium #1 presents the worst quality of surface, with a roughness variation of ±5.5 µm. The surface seems covered by an artificial and brittle ceramic layer so that Li grain boundaries are not visible. For Lithium #2, a surface roughness variation of ±4.5 µm is observable with large furrows in the same direction as the lamination marks. In addition, Li grain boundaries are still visible under these large furrows that suppose a thick layer of lubricant or polymer is applied during the lamination process. This hypothesis seems supported by electrochemical results showing high interfacial resistance for this Li metal.

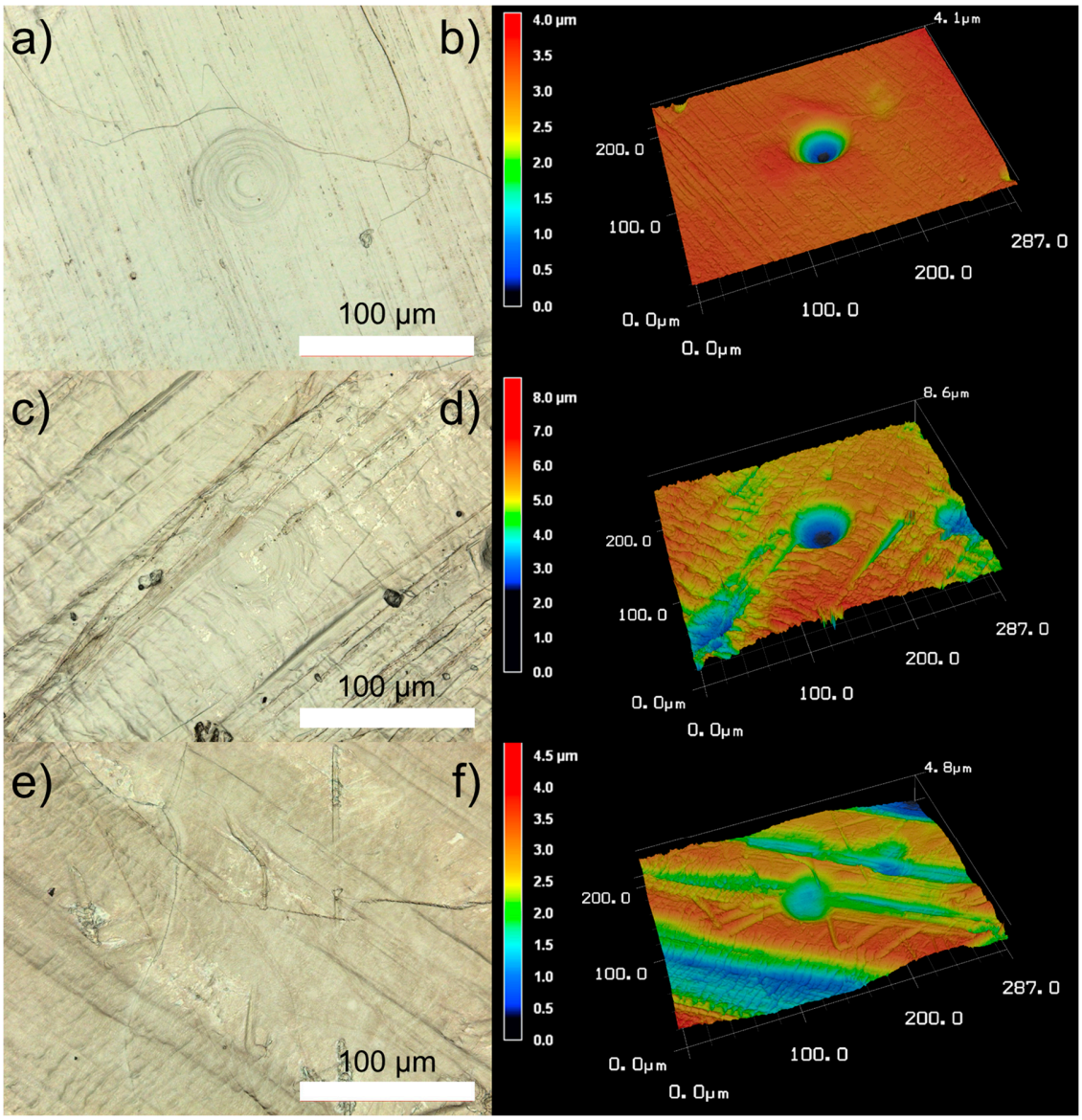

Figure S5. a,c,e) Optical and b,d,f) 3D laser scanning confocal images of a,b) Lithium HQ, c,d) Lithium #1 and e,f) Lithium #2 surfaces. Indentation marks are visible in the middle.

Figure S6 presents the inverse pole figures obtained from EBSD analysis for a) Lithium HQ and b) Lithium #2. Due to the thick ceramic layer on the Lithium #1 surface, EBSD analysis was impossible for this sample. The maps show the crystallographic orientation of Li grains as well as their size/form for each Li metal. It is worth noting that larger Li

grains were obtained for Lithium #2. A graph showing the cumulative number of Li grains as a function of Li grain diameter for Lithium HQ and Lithium #2 is presented in Figure S7a. On the surface analyzed, more than one thousand grains inferior to 1000 µm in diameter are observed for Lithium HQ against ~380 grains for Lithium #2. Figure S7b presents the cumulative percentage of Li grains as a function of Li grain diameter for the two Li foils. The average (Avg), minimum (Min) and maximum (Max) diameters of Li grains for each Li foil are also indicated. For instance, 50% of Li grains are inferior to 83 and 185 µm for Lithium HQ and Lithium #2, respectively.

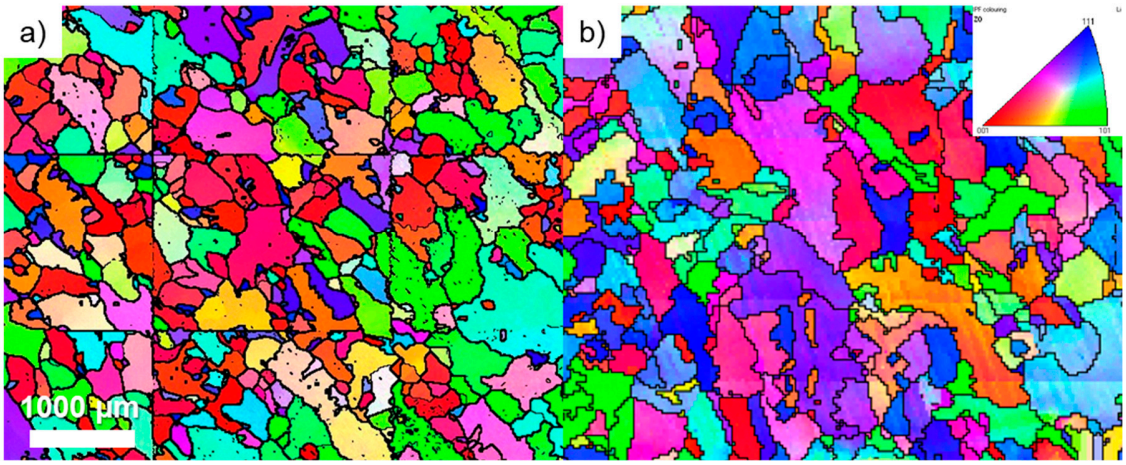

Figure S6. Crystallographic orientation of grains in inverse pole figures (IPF) in the z-axis obtained from EBSD analysis for a) Lithium HQ and b) Lithium #2. Acquisition was impossible for lithium #1 due to the poor surface quality.

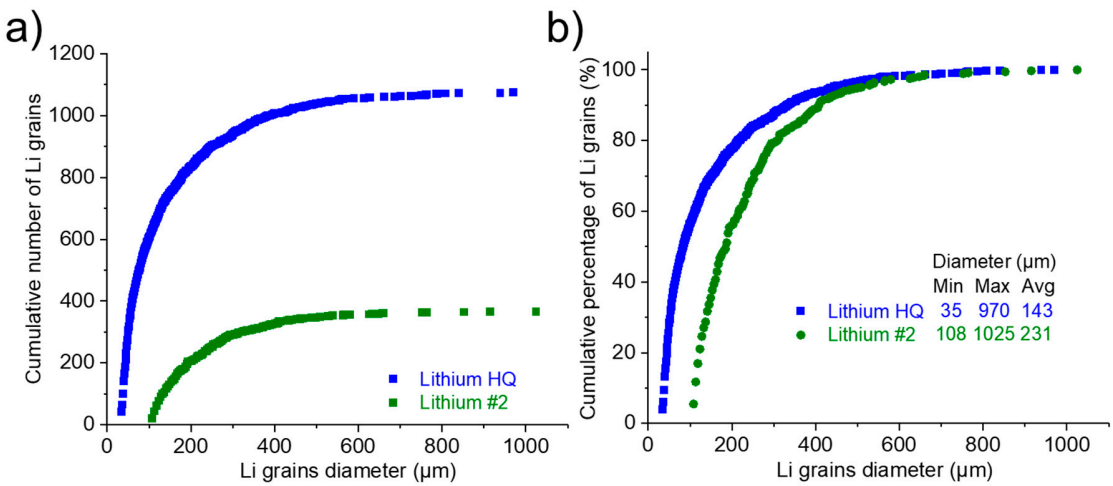

Figure S7. a) Cumulative number of Li grains as a function of Li grain diameter for Lithium HQ and Lithium #2. b) Cumulative percentage of Li grains as a function of Li grain diameter for Lithium HQ and Lithium #2. The average (Avg), minimum (Min) and maximum (Max) diameters of Li grains for each Li foil are given. Data is collected from EBSD inverse pole figure (IPF) maps.

The electrochemical impedance spectra after stabilization for cells made with Lithium HQ, Lithium #1 and Lithium #2 foils exposed in dry room for different time periods are presented in Figures S8, S9 and S10, respectively.

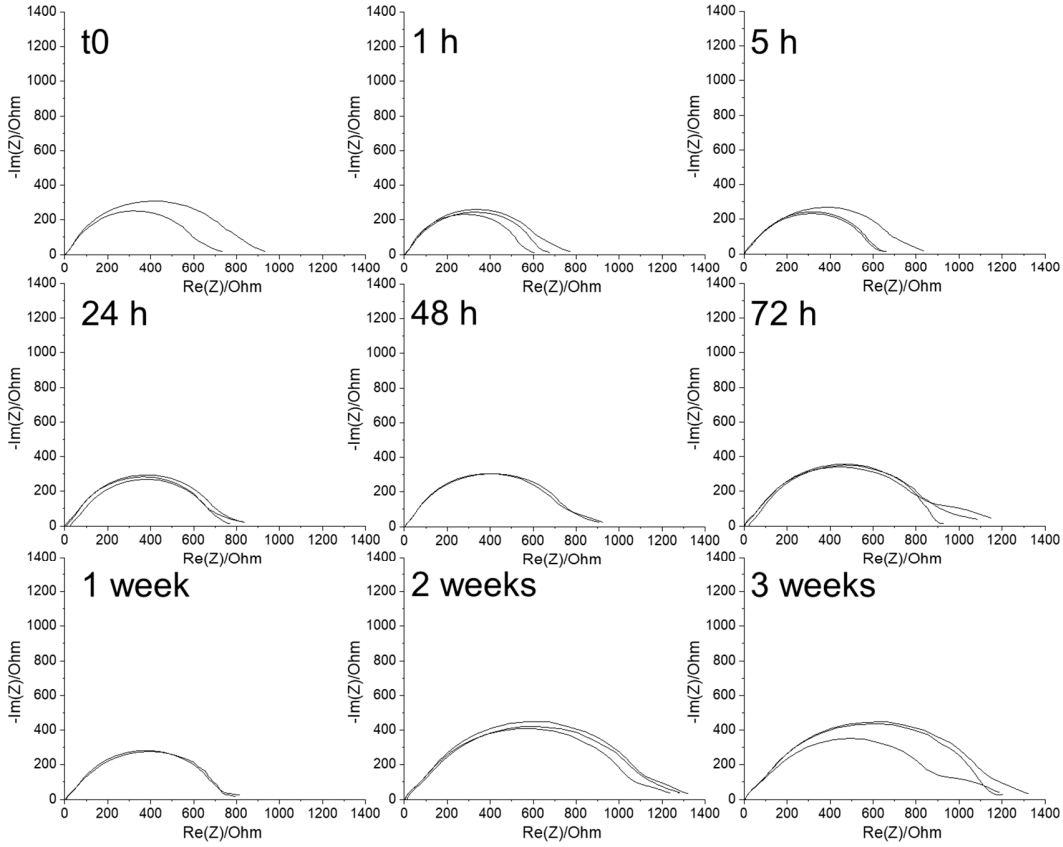

Figure S8. Electrochemical impedance spectra, after stabilization, recorded for cells made with Lithium HQ foils exposed in dry room atmosphere for different time periods.

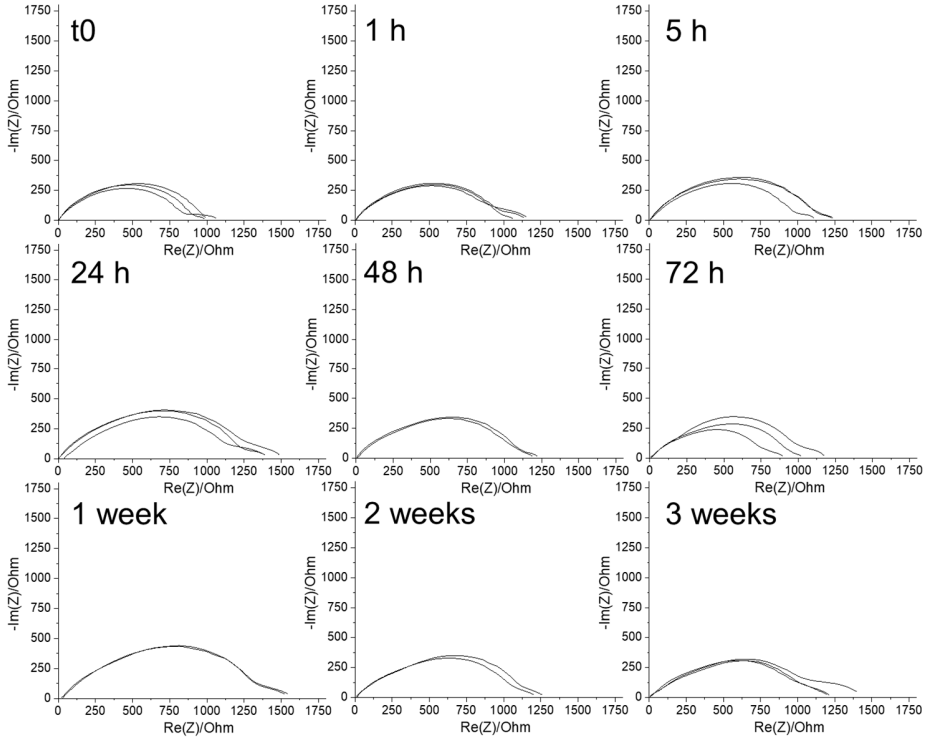

Figure S9. Electrochemical impedance spectra, after stabilization, recorded for cells made with Lithium #1 foils exposed in dry room atmosphere for different time periods.

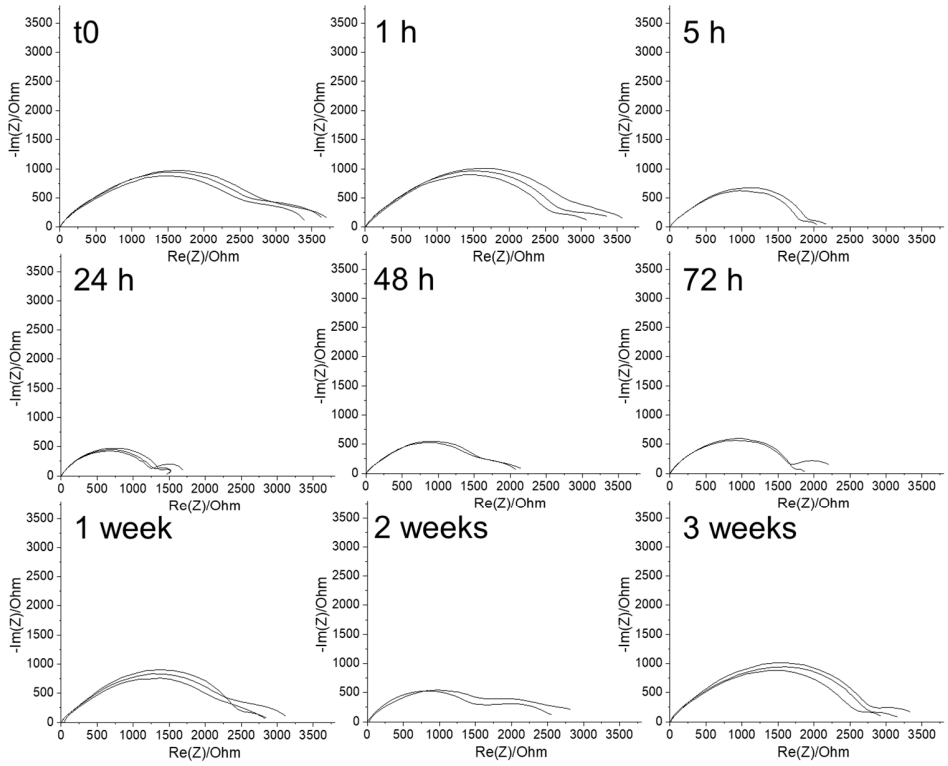

Figure S10. Electrochemical impedance spectra, after stabilization, recorded for cells made with Lithium #2 foils exposed in dry room atmosphere for different time periods.

Galvanostatic stripping-plating cycling for cells made with Lithium HQ, Lithium #1 and Lithium #2 foils exposed in dry room for different time periods are presented in Figures S11, S12 and S13, respectively.

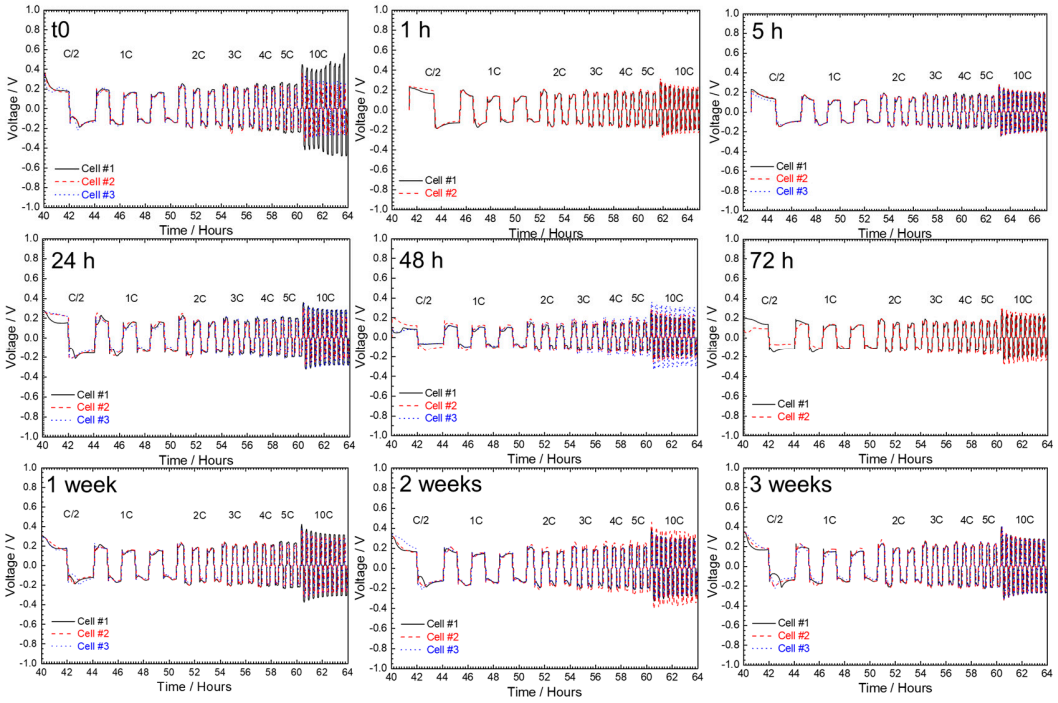

Figure S11. Results of galvanostatic stripping/plating cycling experiment for cells made with Lithium HQ foils exposed in dry room atmosphere for different time periods.

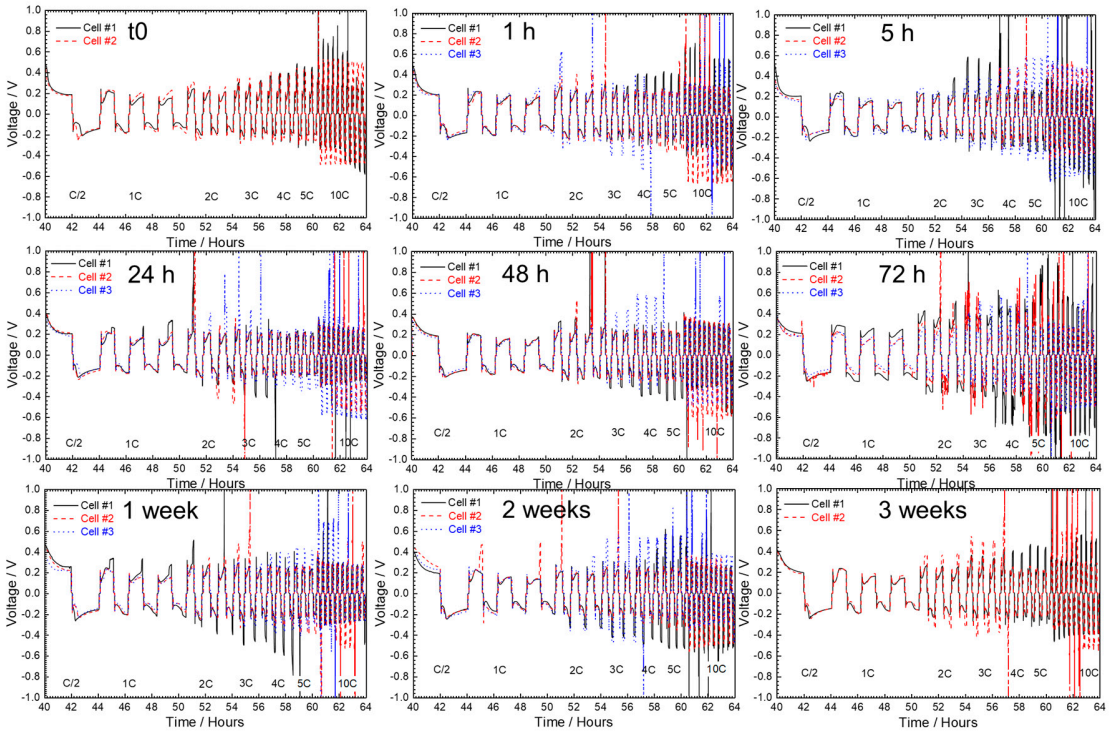

Figure S12. Results of galvanostatic stripping/plating cycling experiment for cells made with Lithium #1 foils exposed in dry room atmosphere for different time periods.

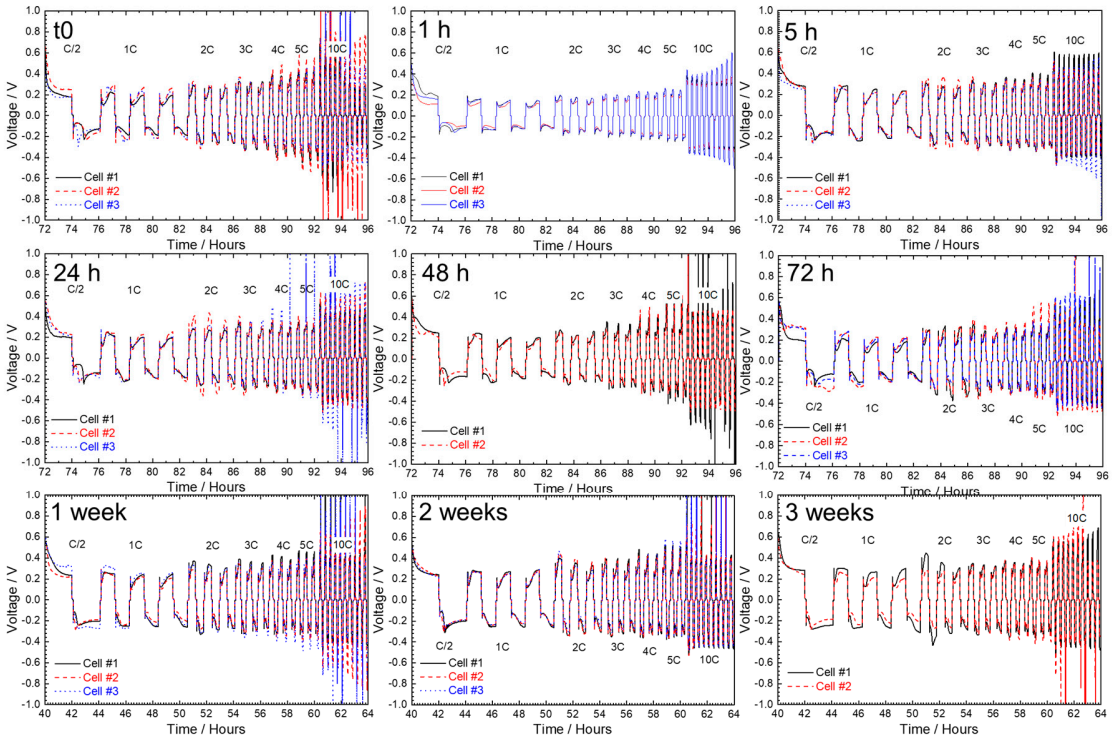

Figure S13. Results of galvanostatic stripping/plating cycling experiment for cells made with Lithium #2 foils exposed in dry room atmosphere for different time periods.

Long-cycling at 2C for cells made with Lithium HQ, Lithium #1 and Lithium #2 foils exposed in dry room for different time periods are presented in Figures S14, S15 and S16, respectively.

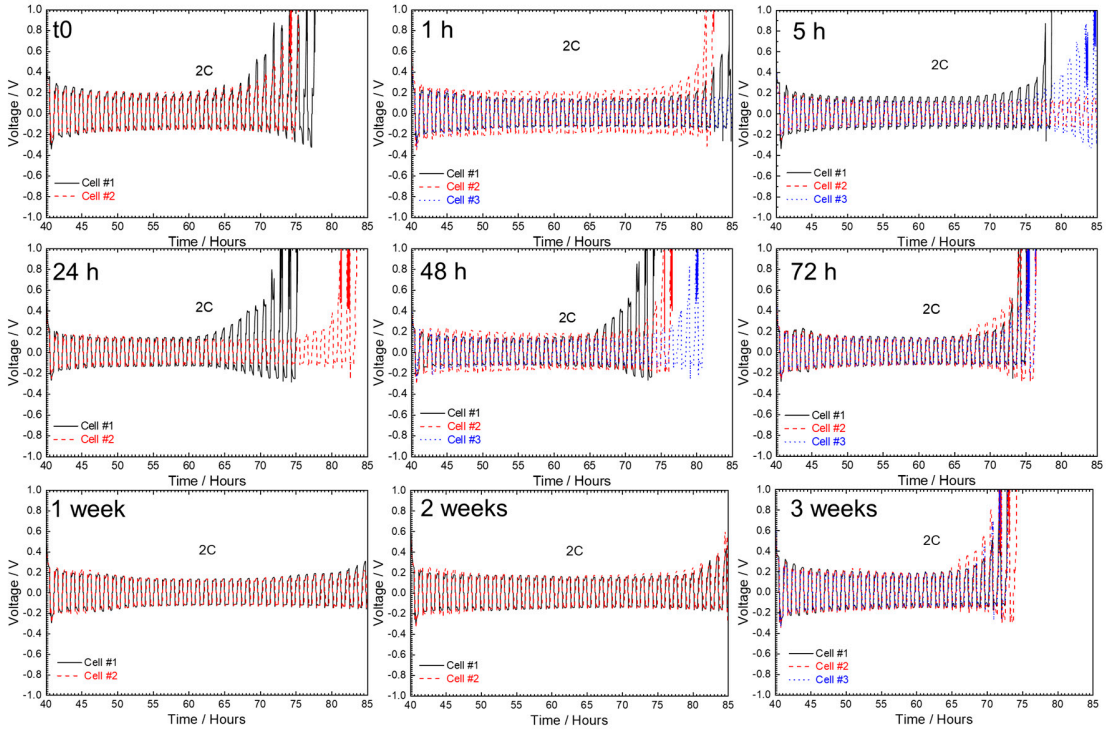

Figure S14. Results of long-cycling experiment at 2C for cells made with Lithium HQ foils exposed in dry room atmosphere for different time periods.

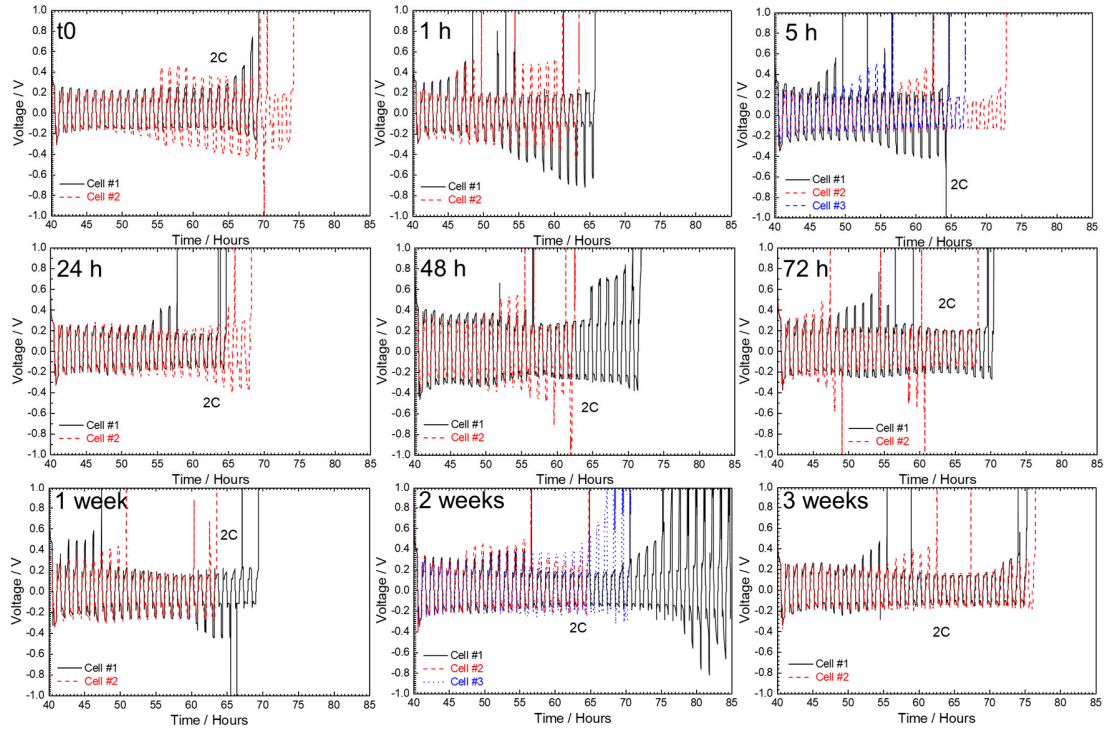

Figure S15. Results of long-cycling experiment at 2C for cells made with Lithium #1 foils exposed in dry room atmosphere for different time periods.

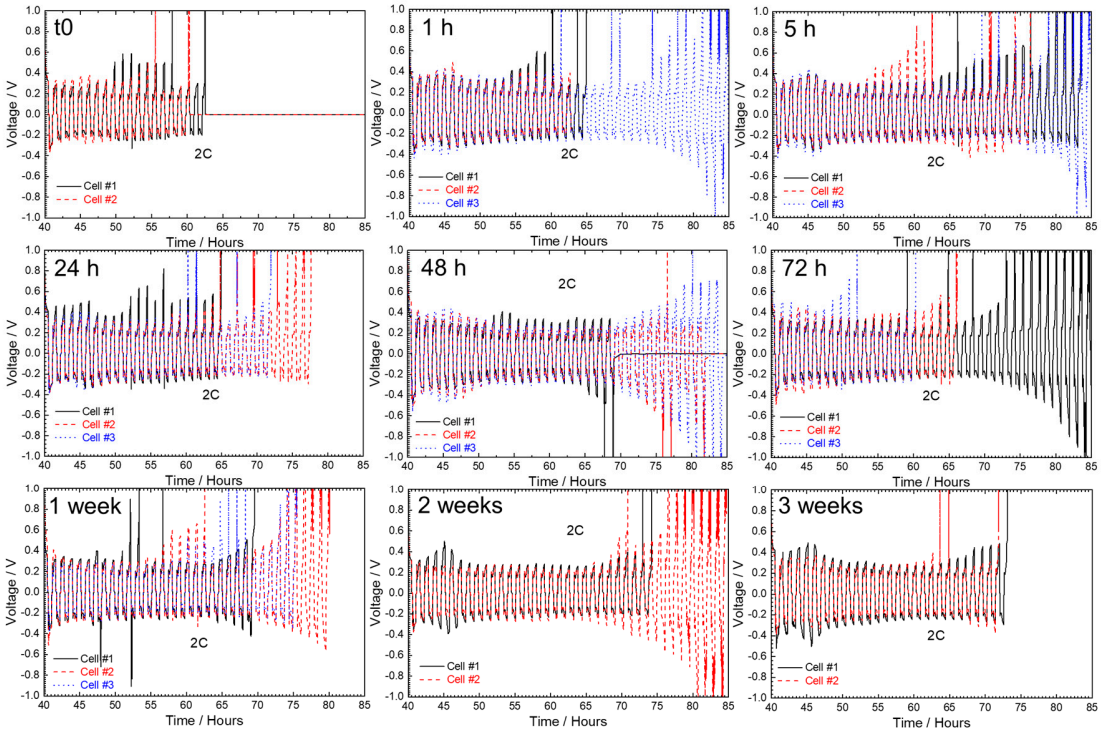

Figure S16. Results of long-cycling experiment at 2C for cells made with Lithium #2 foils exposed in dry room atmosphere for different time periods.